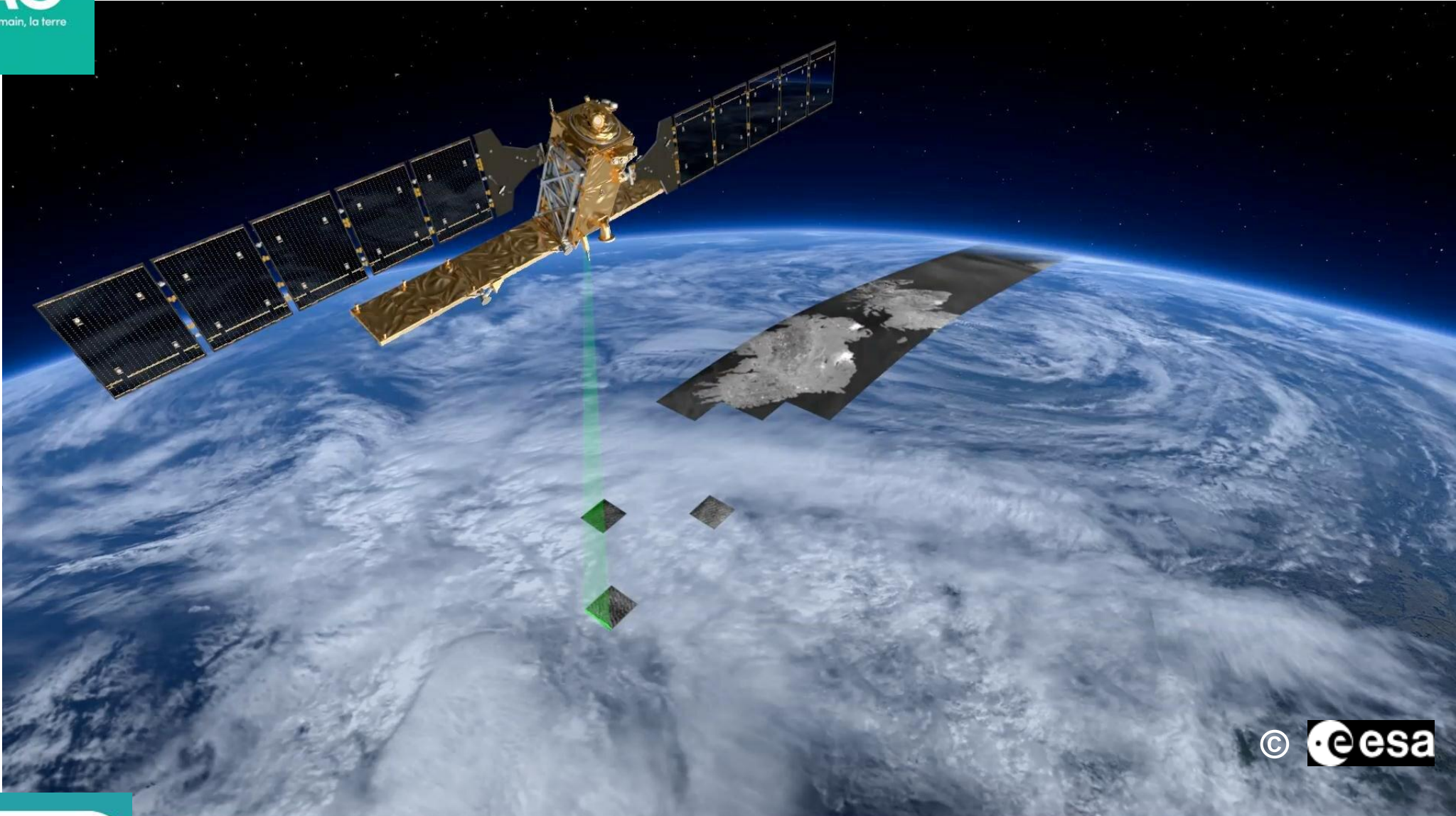


SAR images acquisition and processing



© esa

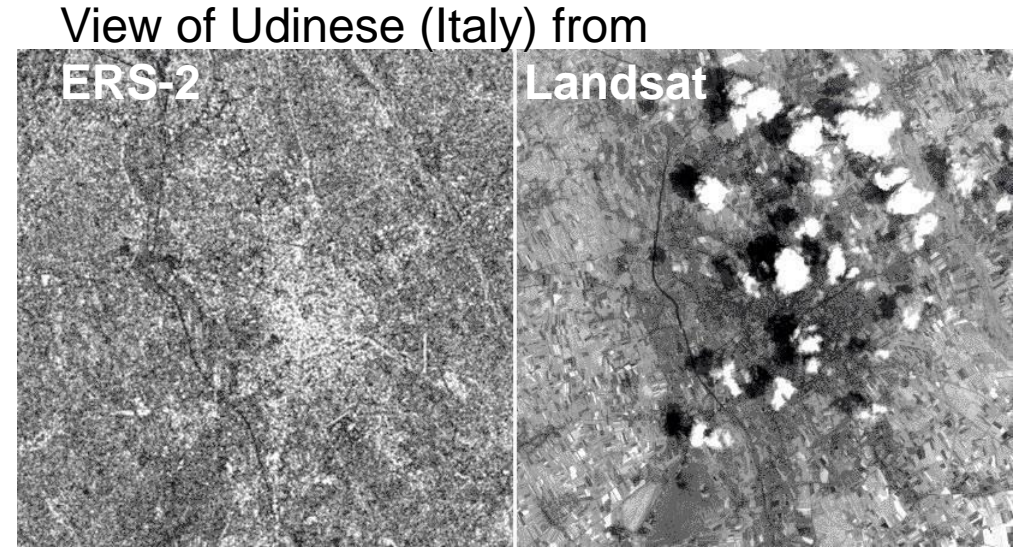
Outline

- ❖ **Introduction**
- ❖ **Types of radar acquisitions**
- ❖ **Real Aperture Radar (RAR) images**
- ❖ **Synthetic Aperture Radar (SAR) images**
- ❖ **SAR images acquisition**
- ❖ **SAR images processing**

Introduction

Interest of radar images

- ❖ **Independence of solar illumination**
 - ⇒ can be acquired night and day



<https://earth.esa.int/eogateway/missions/ers/radar-courses/radar-course-2>

Interest of radar images

- ❖ **Independence of solar illumination**
⇒ can be acquired night and day
- ❖ **Independence of weather conditions**
⇒ much longer wavelengths than optical or IR
microwaves easily penetrate clouds



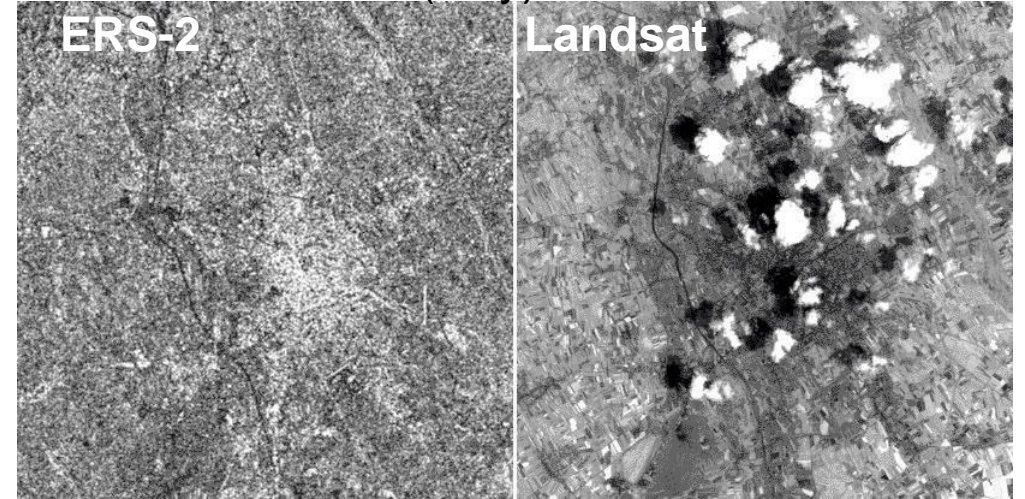
Presence of convective raincells
can be observed on images
acquired at C and X bands

Example: Two Sentinel-1 (C-band) from
20/10/2018 (left) and 13/11/2018 (right)
displayed in RGB: VV, VH, NDI(VV,VH) over Congo

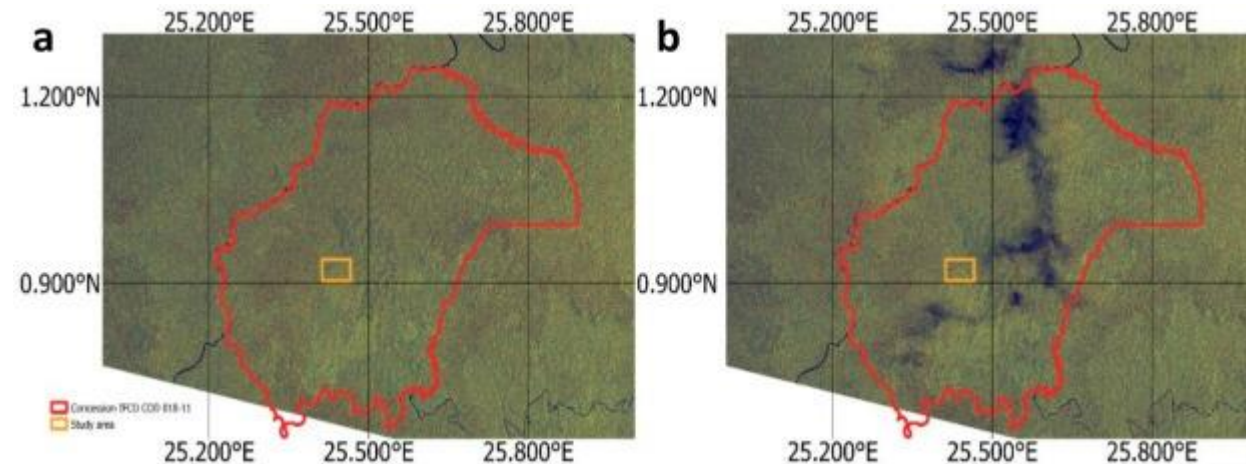
Ygorra et al. (2021). Monitoring loss of tropical
forest cover from Sentinel-1 time-series.

International Journal of Applied Earth Observation and Geoinformation, 103, 102532.

View of Udinese (Italy) from



<https://earth.esa.int/eogateway/missions/ers/radar-courses/radar-course-2>



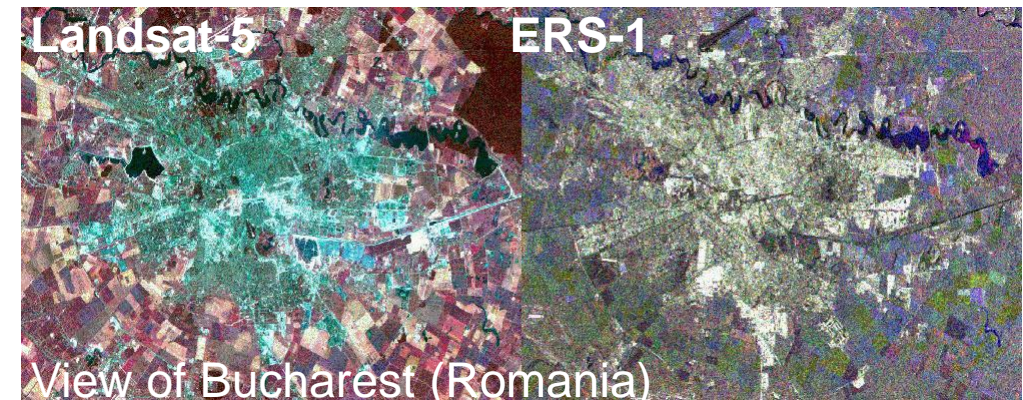
Interest of radar images

- ❖ **Control of emitted electromagnetic radiation**
 - ⇒ properties of EM radiation
(power, frequency, polarisation)
optimised according to specific goals



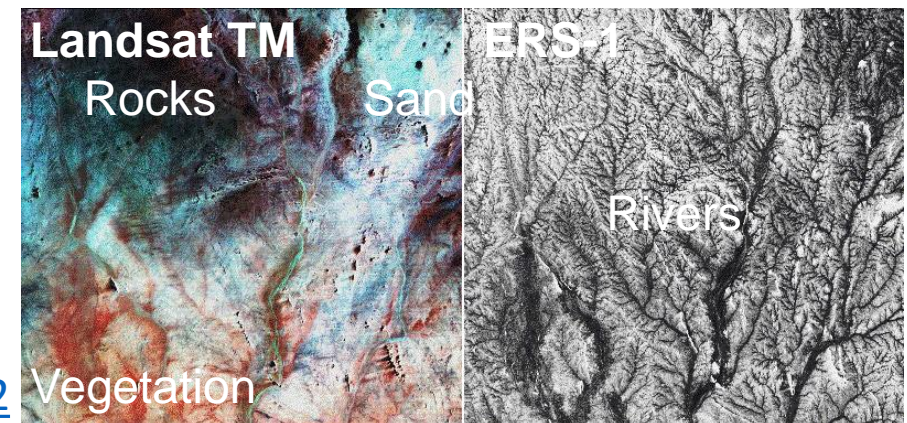
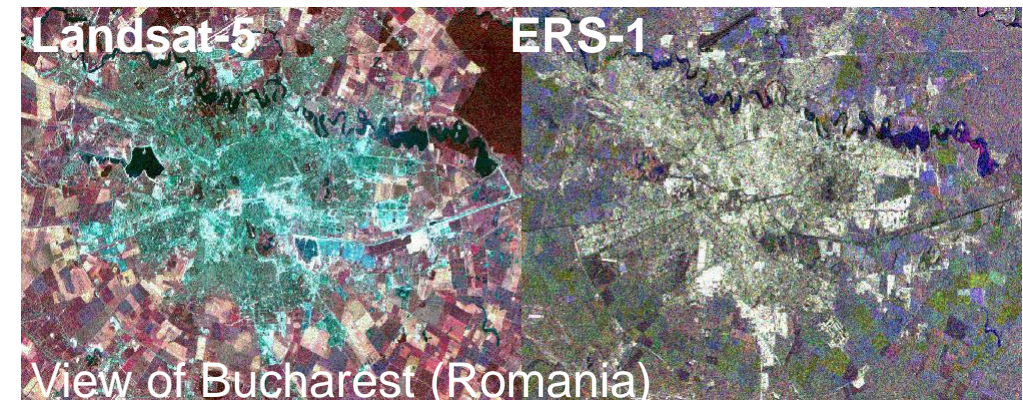
Interest of radar images

- ❖ **Control of emitted electromagnetic radiation**
 - ⇒ properties of EM radiation (power, frequency, polarisation) optimised according to specific goals
- ❖ **Control of imaging geometry**
- ❖ **Access to different parameters compared to optical systems**
 - ⇒ optical: surface layer (i.e., colour) vs. microwave: geometric and dielectric properties of the surface or volume (i.e., roughness)



Interest of radar images

- ❖ **Control of emitted electromagnetic radiation**
 - ⇒ properties of EM radiation (power, frequency, polarisation) optimised according to specific goals
- ❖ **Control of imaging geometry**
- ❖ **Access to different parameters compared to optical systems**
 - ⇒ optical: surface layer (i.e., colour) vs. microwave: geometric and dielectric properties of the surface or volume (i.e., roughness)
- ❖ **Access to information about subsurface features**
 - Longer λ ⇒ penetration of soil, sand, snow in very dry conditions only, forest canopy



Types of radar acquisitions

Radar types

- ❖ Scatterometers

- ❖ Altimeters

- ❖ Radar imaging systems

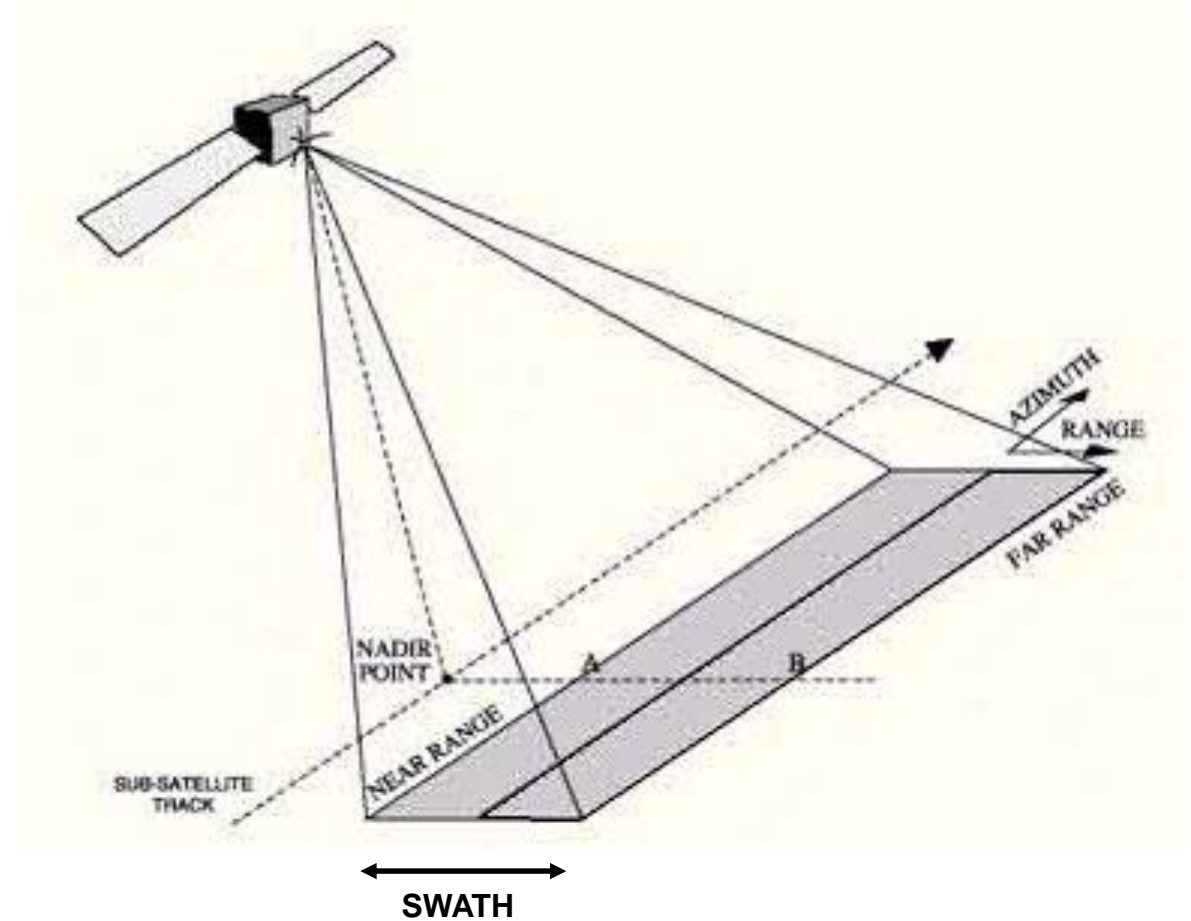
- Real Aperture Radar (RAR)

- Synthetic Aperture Radar (SAR)

Both RAR and SAR are side-looking systems

with an illumination direction

usually perpendicular to the flight line.



Radar images

Short (microsecond) high energy pulses are emitted and the returning echoes recorded, providing information on:

- ❖ magnitude**
- ❖ phase**
- ❖ time interval between pulse emission and return from the object**
- ❖ polarization**
- ❖ Doppler frequency**

Real Aperture Radar (RAR) images

Radar images from RAR

- ❖ RAR or SLAR (Side Looking Airborne Radar)
- ❖ azimuth resolution determined by the antenna beamwidth
- ❖ Range resolution (across-track)
- To be distinguishable, two targets must be separated by the distance:

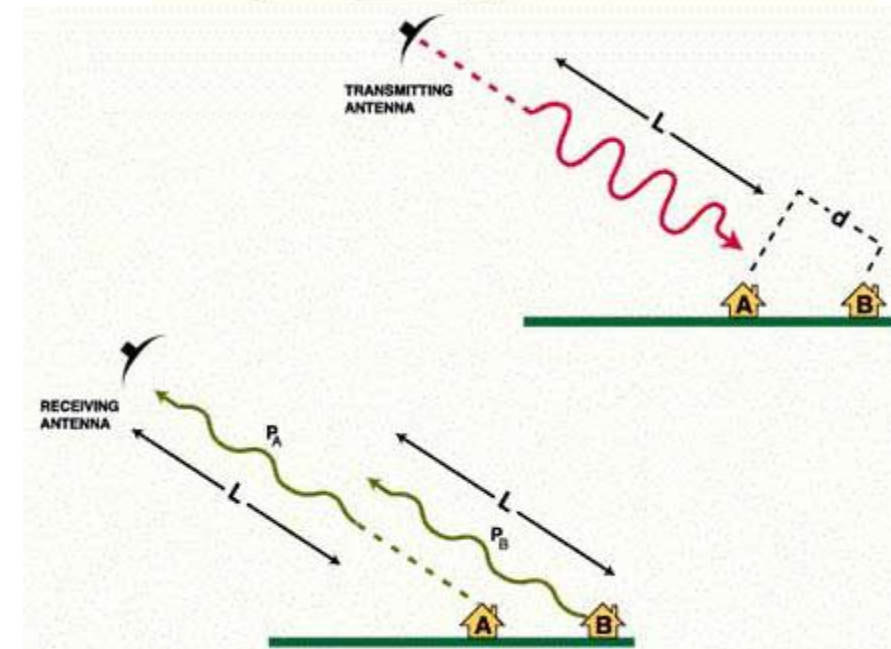
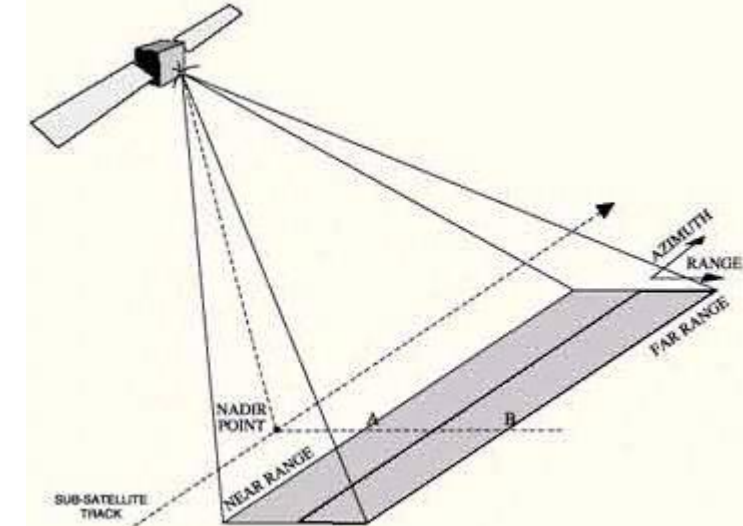
$$d > L / 2$$

where L is the length of the pulse

$$L = c\tau$$

where τ is the duration of the pulse

$$\Rightarrow d > c\tau / 2$$



Radar images from RAR

❖ Ground range resolution (across-track)

$$d_{\min} = L / 2 = \delta R_s$$

where δR_s : slant range resolution

The ground range resolution (δR_g) is equal to:

$$\delta R_g = \delta R_s / \sin\theta = L / (2 \sin\theta)$$

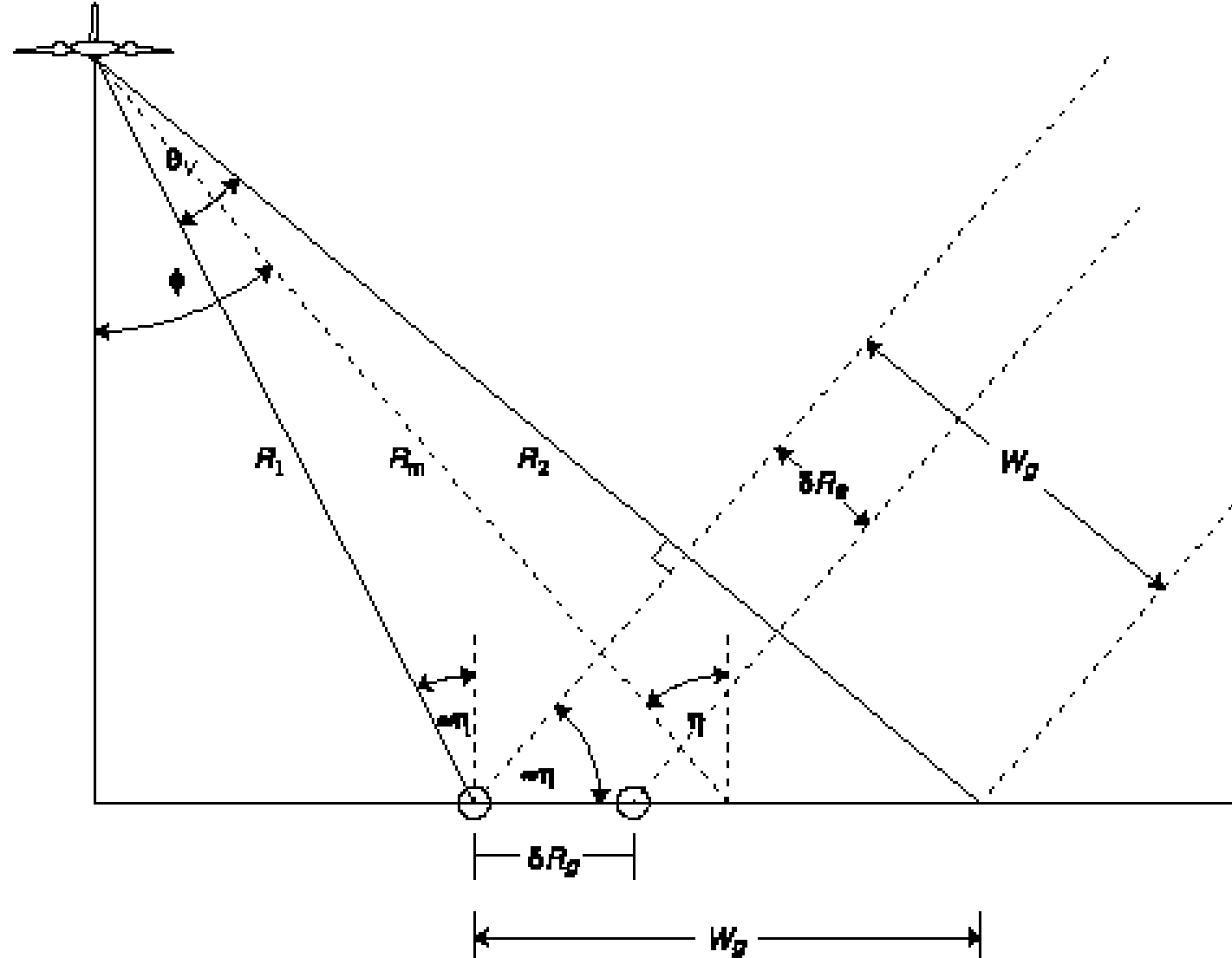
$$\delta R_g = c\tau / (2 \sin\theta)$$

$$\delta R_g = c / (2 B_w \sin\theta)$$

where θ : incidence angle

B_w : bandwidth

If $B_w = 10$ MHz, $\theta = 30^\circ$, $\delta R_g = 7.5$ m



Radar images from RAR

❖ Azimuth resolution (along-track)

Ability of an imaging radar to separate two closely spaced scatterers in the direction parallel to the motion vector

Two objects are in the radar beam simultaneously, for almost all pulses, they both cause reflections, and their echoes will be received at the same time.

Two targets in the azimuth or along-track resolution can be separated only if the distance between them is larger than the radar beamwidth. Hence the beamwidth is taken as the azimuth resolution.

For all types of radars, the beamwidth is a constant angular value with range. For a diffraction limited system, for a given wavelength λ , the azimuth beamwidth b depends on the physical length dH of the antenna in the horizontal direction according to:

$$b = \lambda / dH$$

Radar images from RAR

For example, to obtain a beamwidth of 10 milliradians using 50 millimetres wavelength, it would be necessary to use an antenna 5 metres long. The real aperture azimuth resolution is given by:

$$\text{raz} = Rb$$

with raz: azimuth resolution

R: slant range

For example for a Real Aperture Radar of beamwidth 10 milliradians, at a slant range R equal to 700 kilometres, the azimuth resolution raz will be:

$$\text{raz} = 700 \times 0.01$$

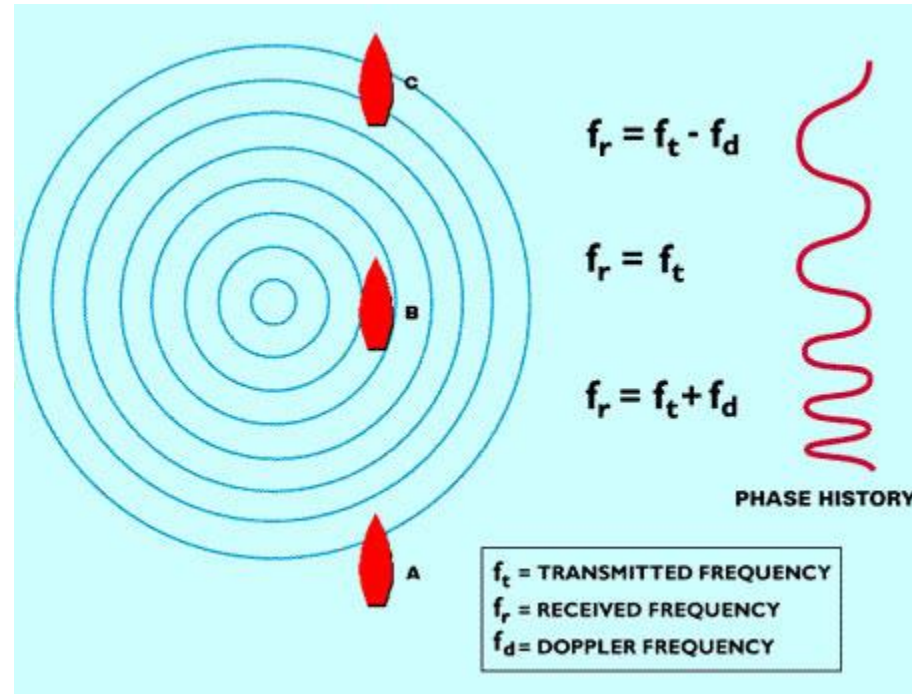
$$\text{raz} = 7 \text{ km}$$

Synthetic Aperture Radar (SAR) images

Radar images from SAR

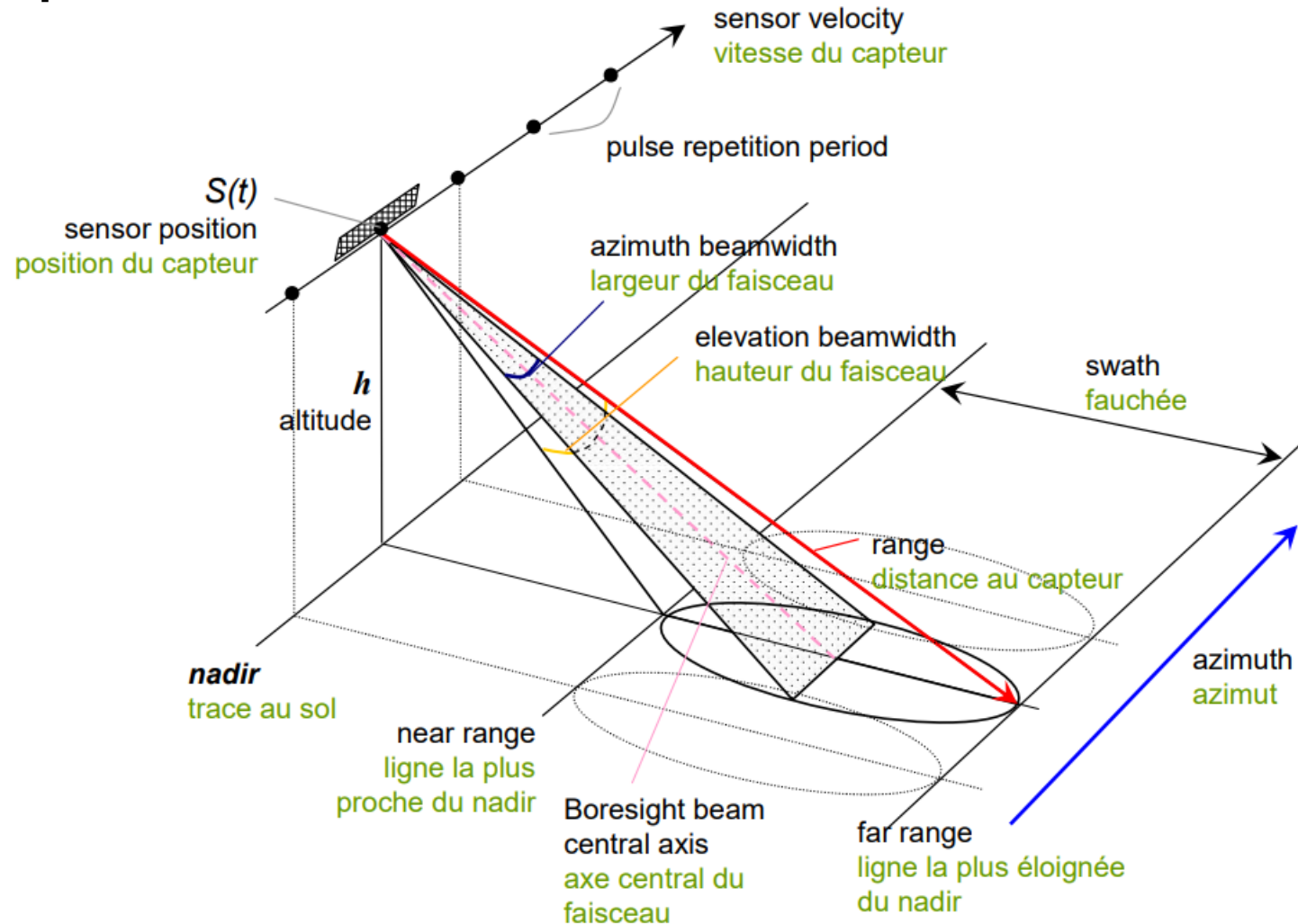
- ❖ **SAR developed to overcome the limitations of RAR.**
i.e., to achieve good azimuth resolution independent of the slant range
yet using small antennae and relatively long wavelengths.

⇒ use of the Doppler effect (motion of the sensor)



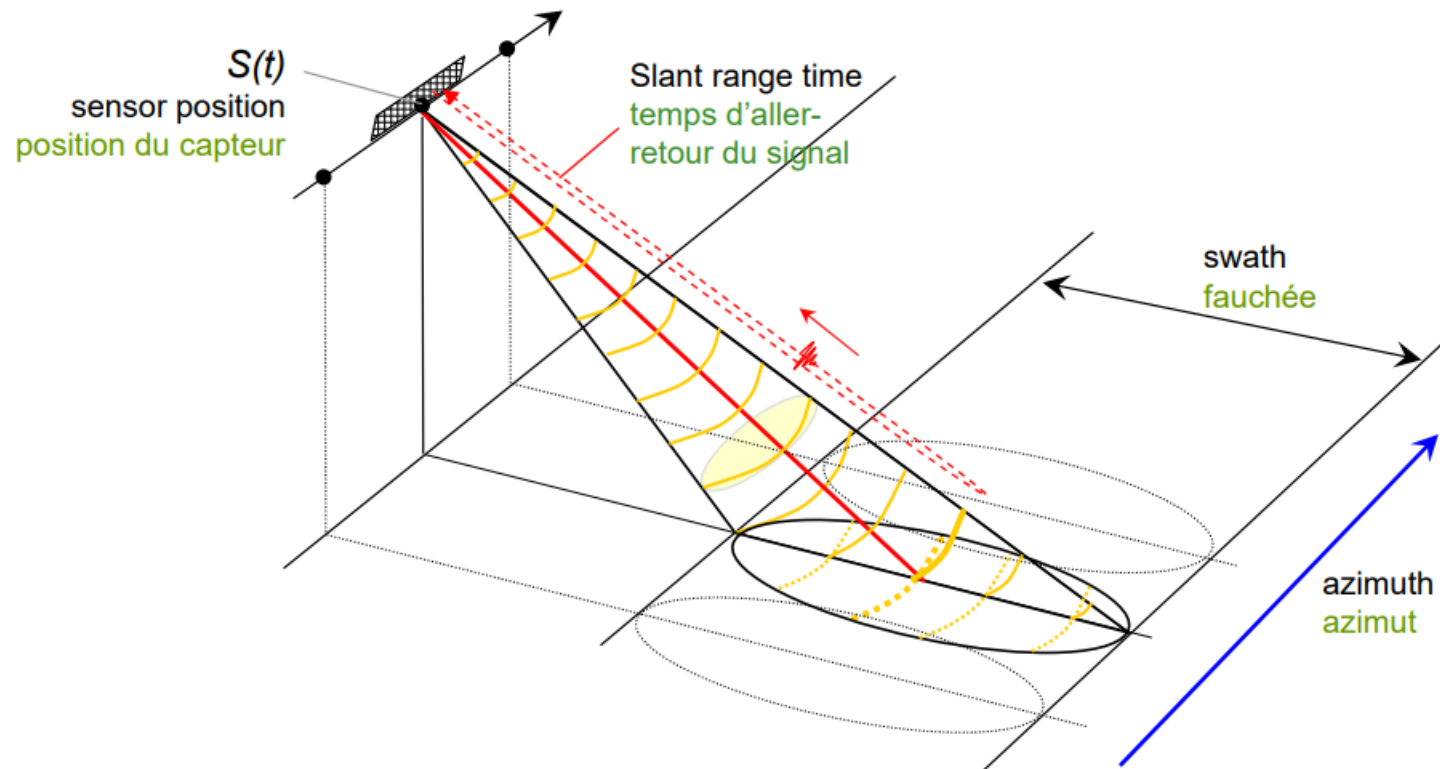
Radar images from SAR

❖ Measurement principle



Radar images from SAR

➤ Range



Radar images from SAR

➤ Azimuth

Observed frequency (f):

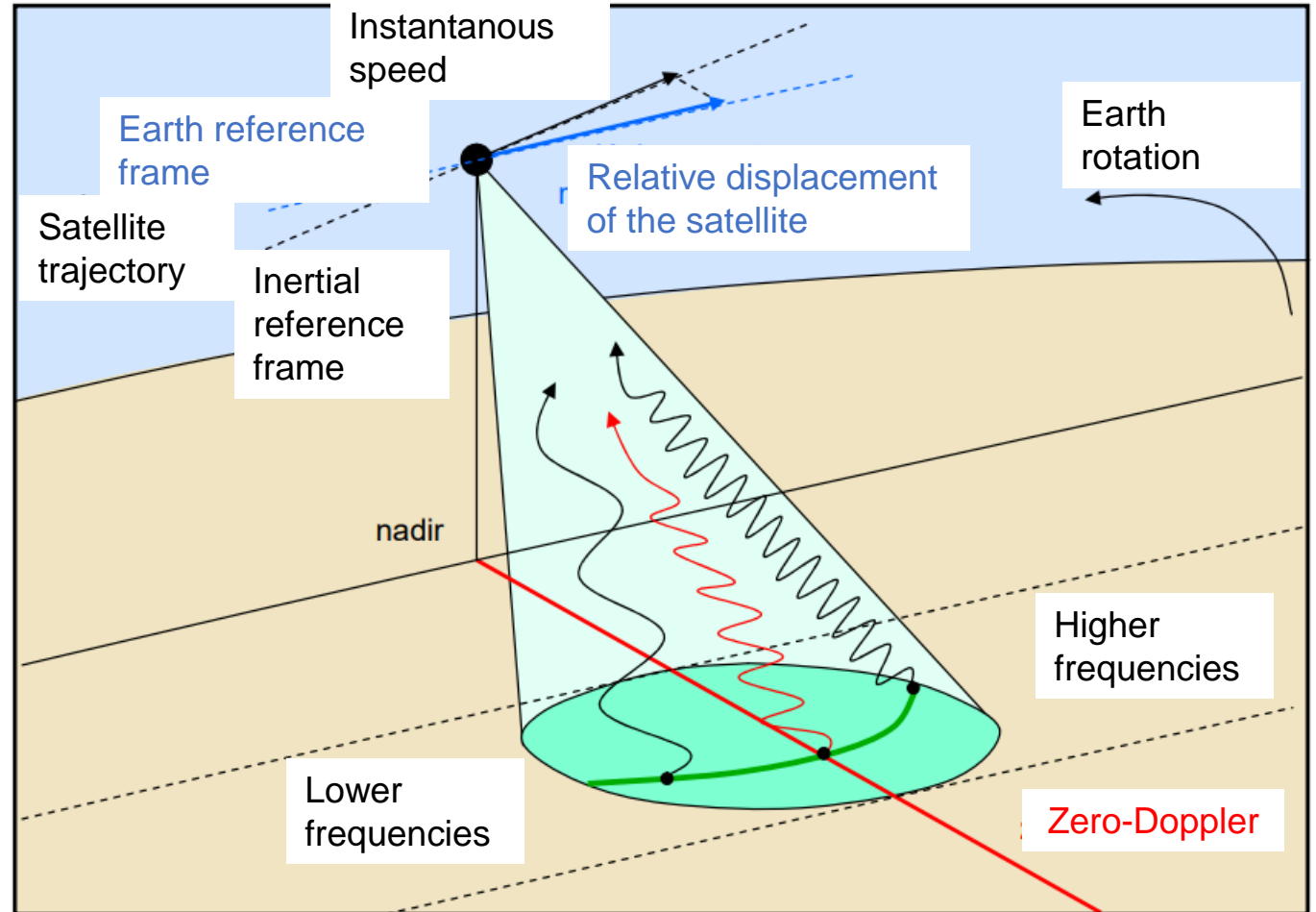
$$f = f_0 \pm \Delta f$$

with f_0 : transmitted frequency
 Δf : change in frequency

$$\Delta f = \Delta v / c \times f_0$$

with $\Delta v = v_s - v_r$

with v_s : velocity of the source
 v_r : velocity of the receiver (= 0 here)



SAR images acquisition

SAR images processing levels

❖ Level-0 Raw Products

❖ Level-1

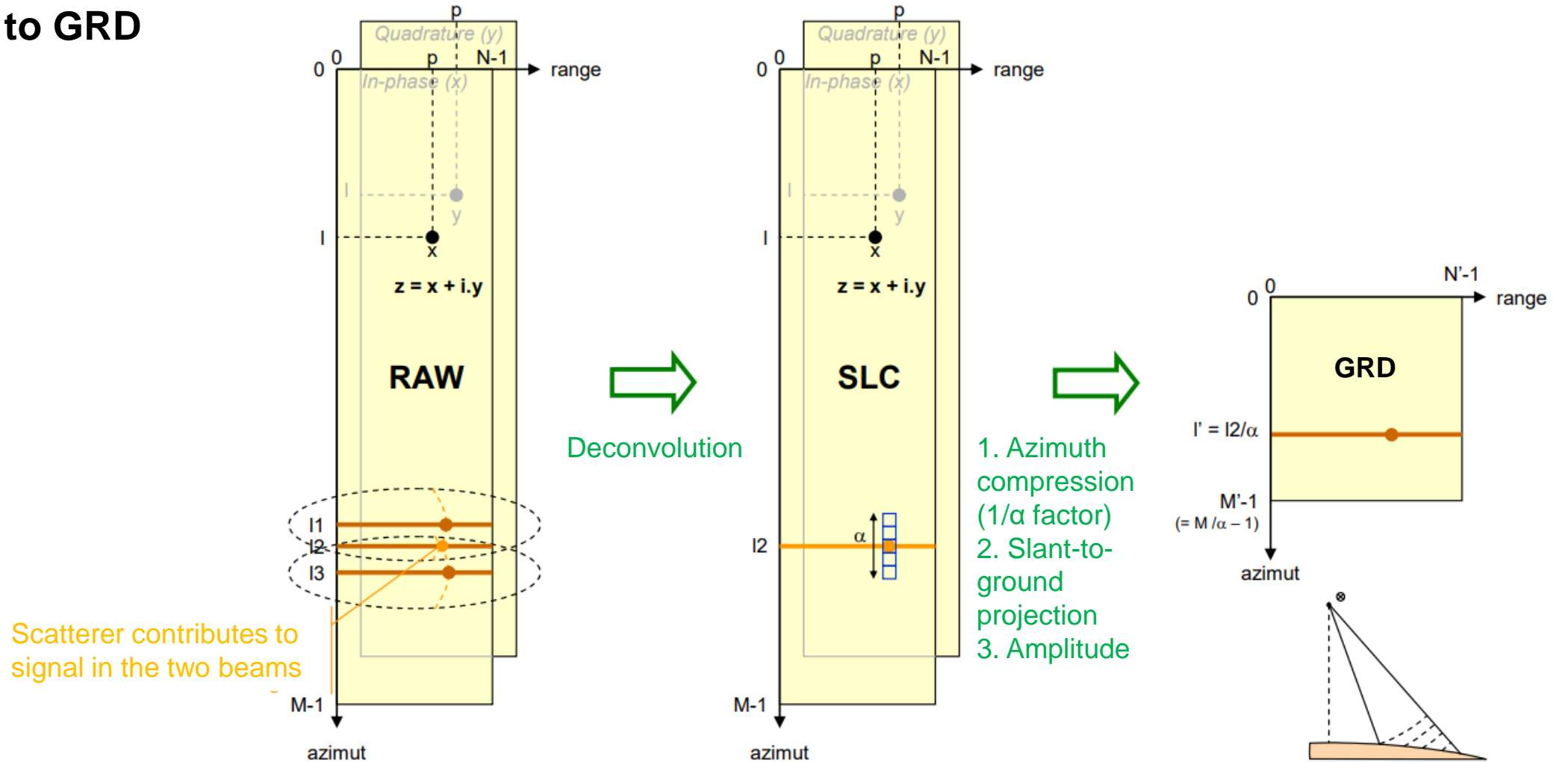
- Single Look Complex (SLC) products
- Ground Range Detected (GRD) products

❖ Level-2

- Ocean Wind field (OWI)
- Ocean Swell spectra (OSW)
- Surface Radial Velocity (RVL)

SAR images processing levels

❖ From RAW to GRD



SAR images processing levels

ERS-2 SAR image from 27/02/1999. View of Napoli (Italy)

❖ RAW

Quadrature
Imaginary part

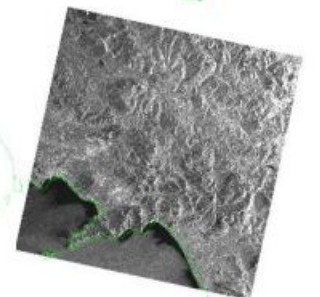
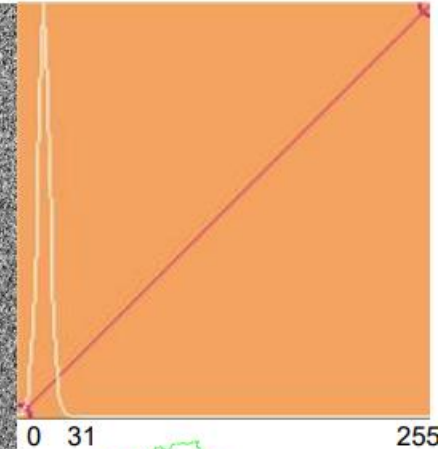
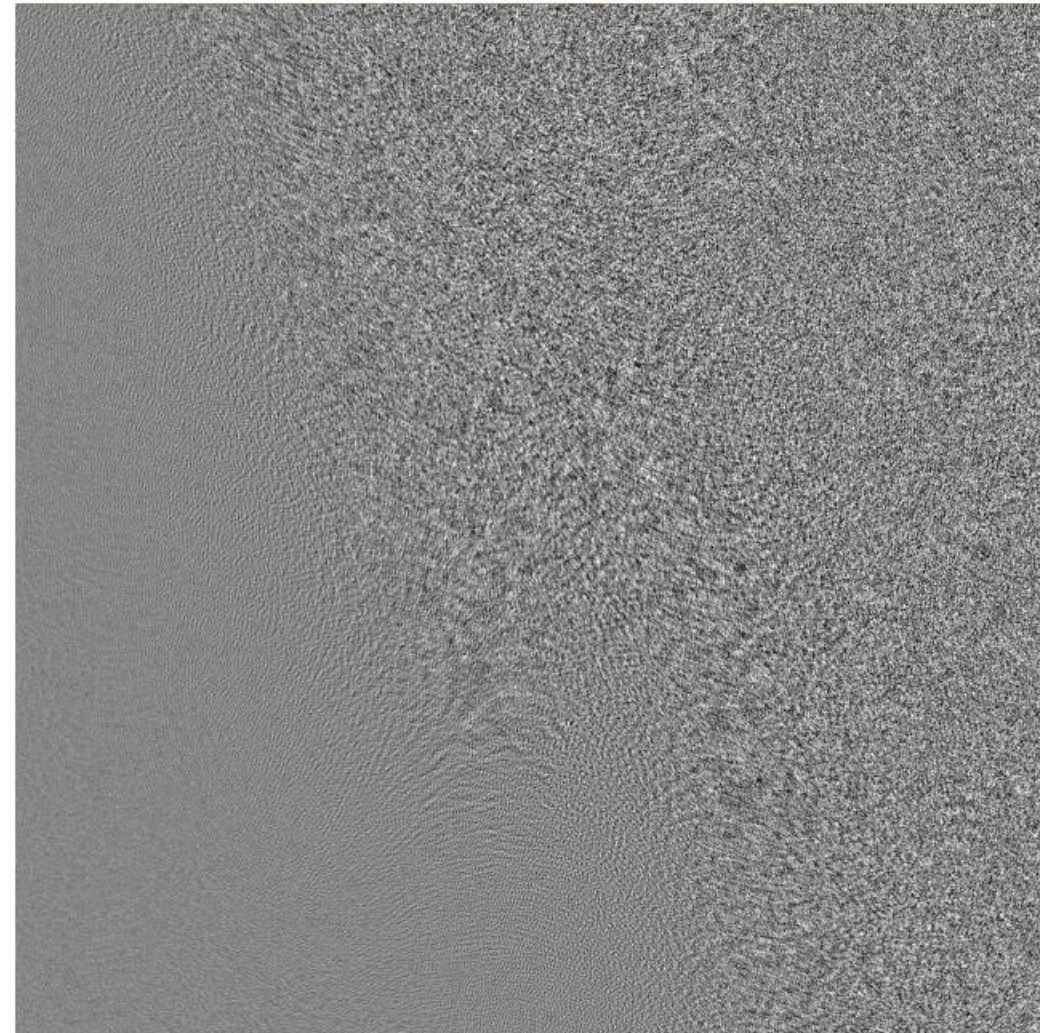
In-phase
Real part

5 unsigned
bytes/pixel

7,904 m
3,978 m

28000

5616



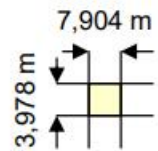
SAR images processing levels

❖ SLC

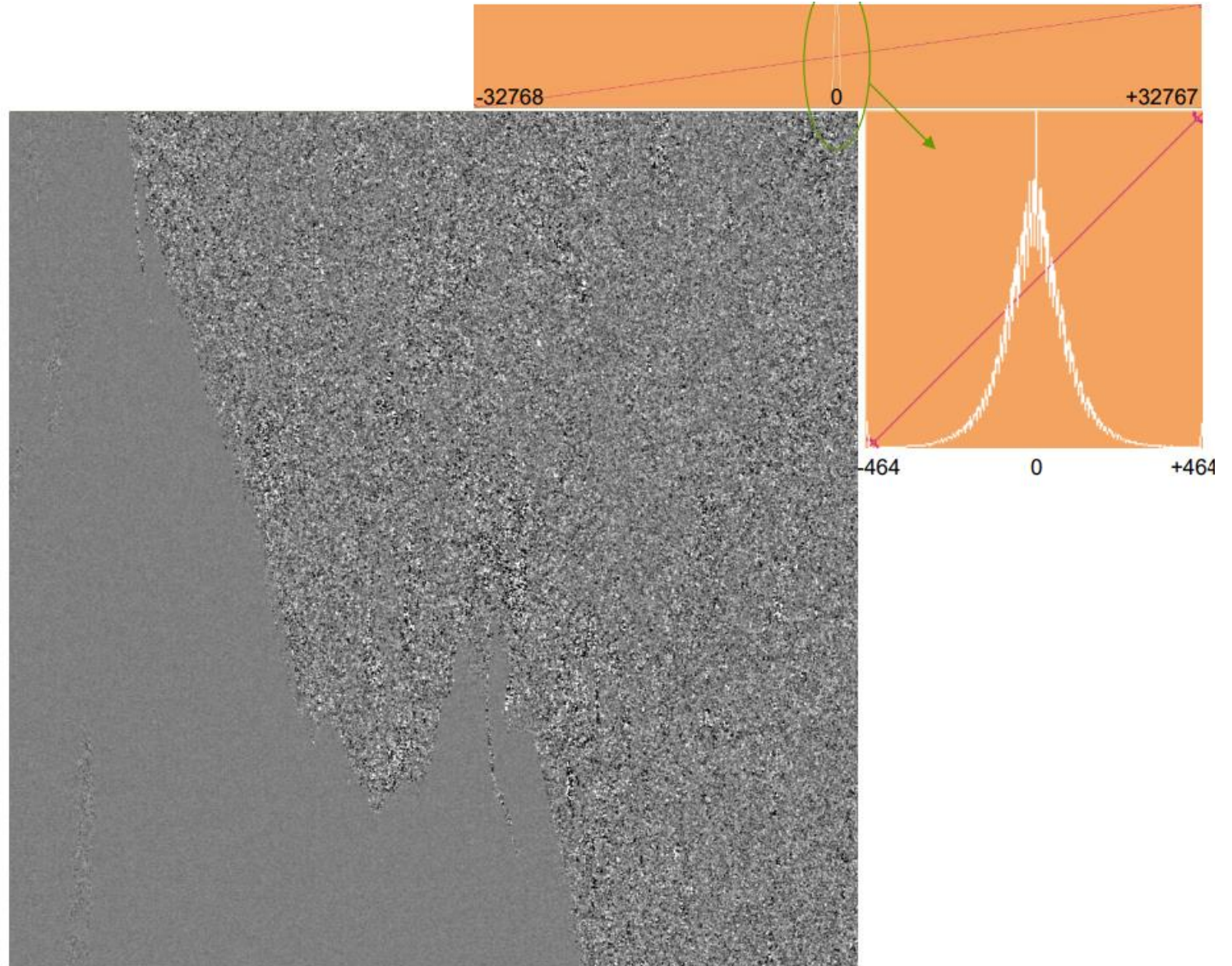
Quadrature
Imaginary part

In-phase
Real part

16 signed
bytes/pixel



26477

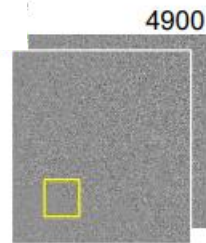


SAR images processing levels

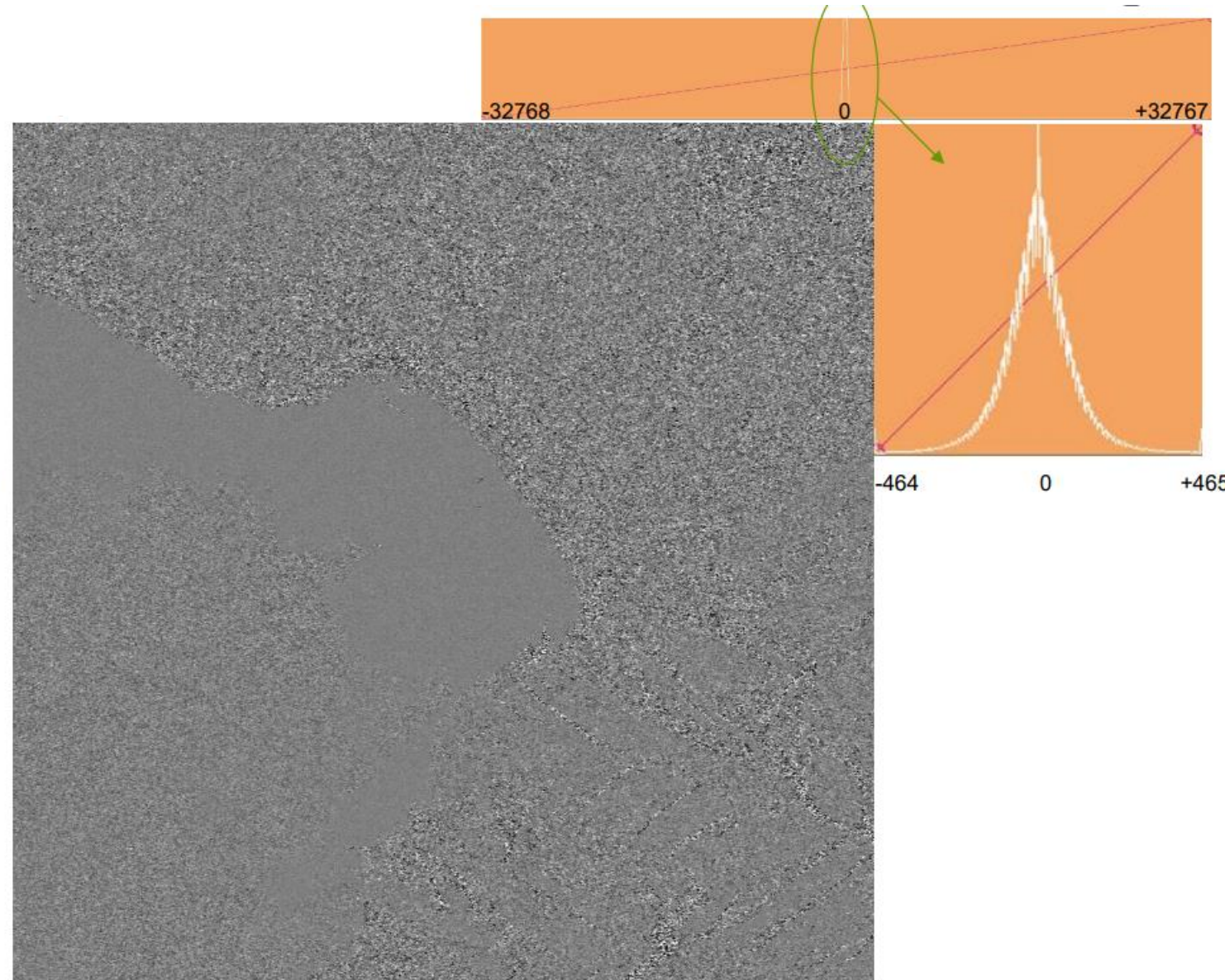
❖ Azimuth-compressed SLC

16 signed bytes/pixel

Quadrature
Imaginary part
In-phase
Real part



19,89 m = 5 x 3,978 m
7,904 m



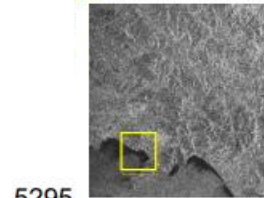
SAR images processing levels

❖ SLC module

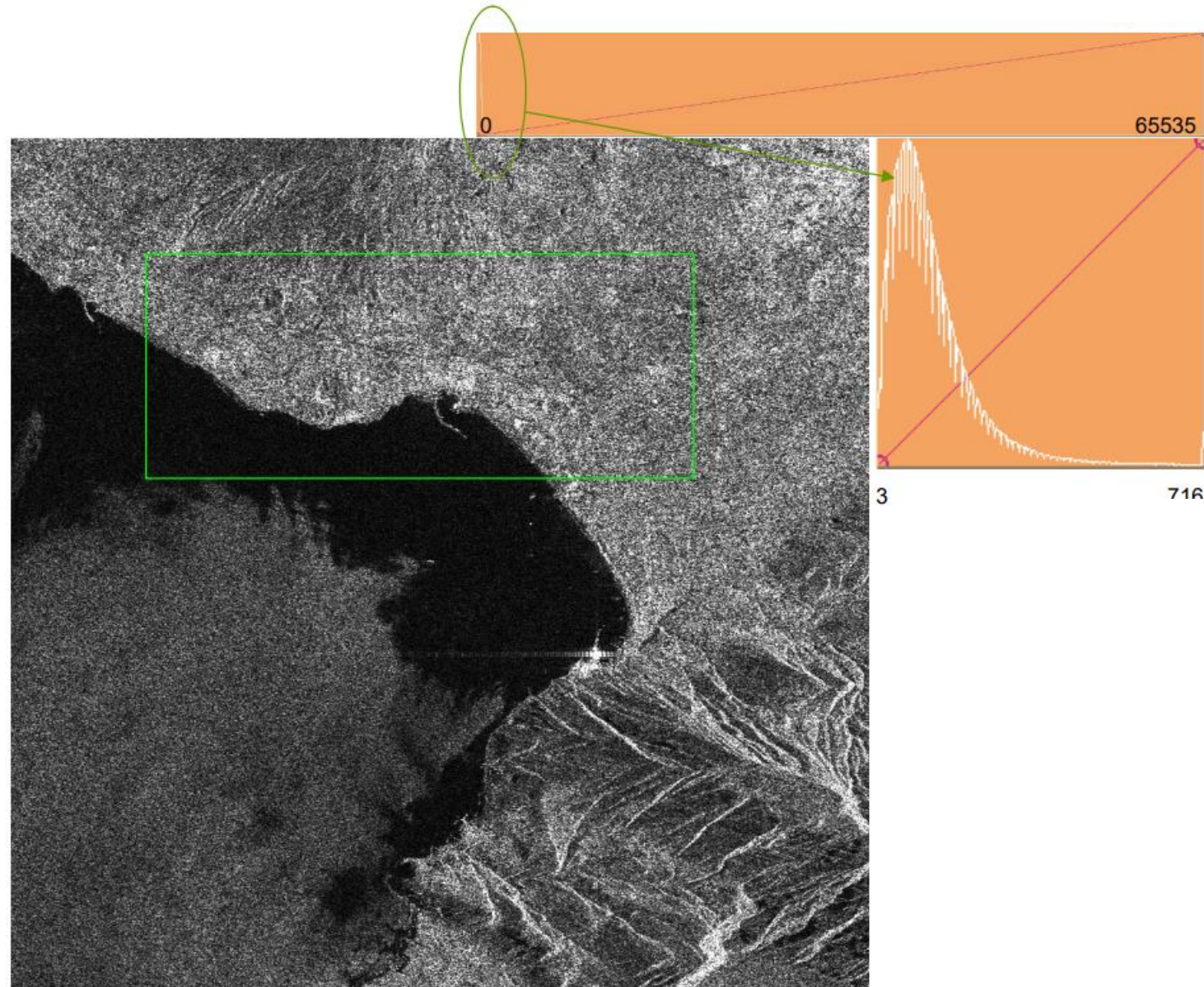
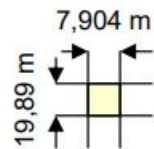
16 unsigned
bytes/pixel

Quadrature
Imaginary part 4900

In-phase
Real part



5295



SAR images processing levels

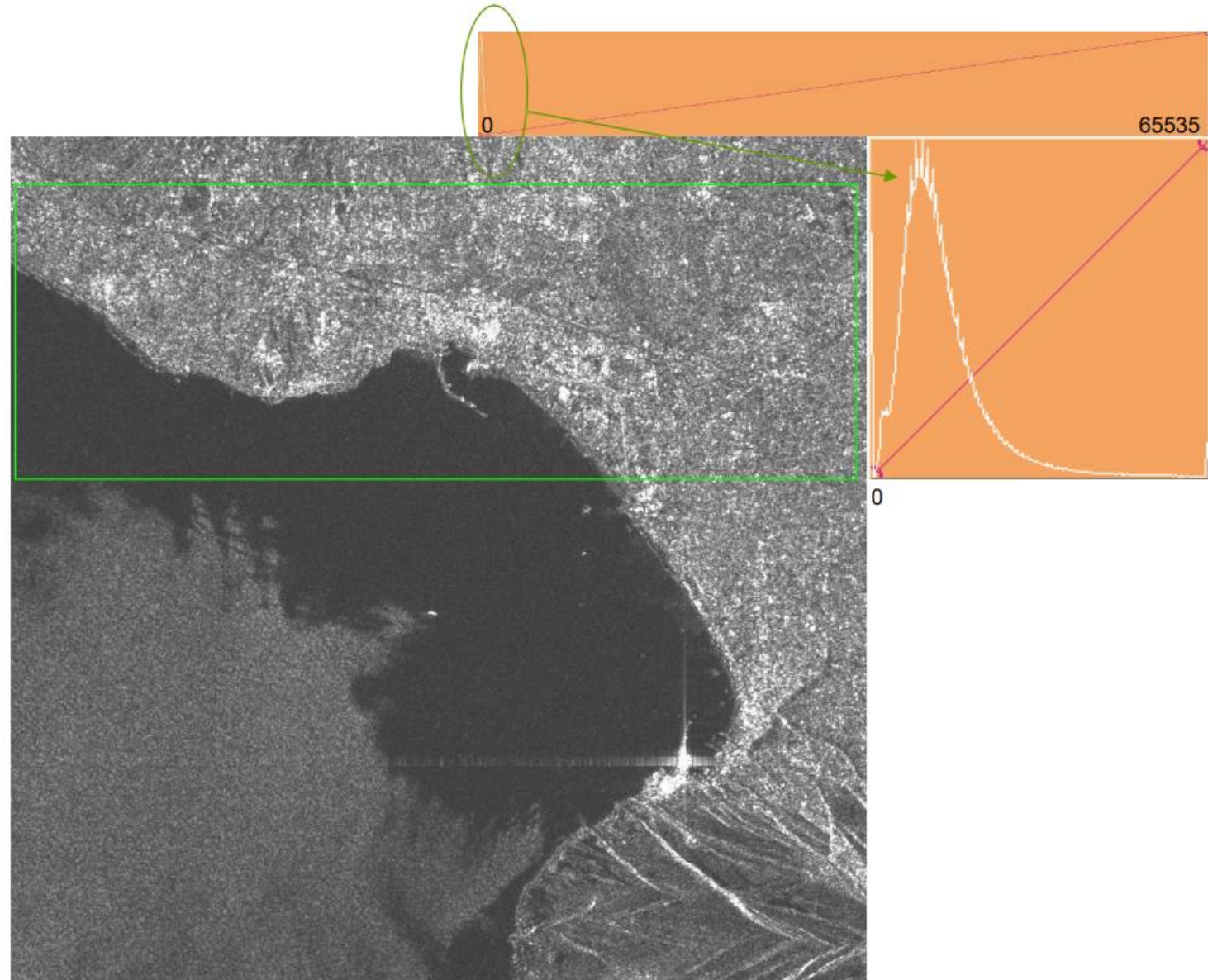
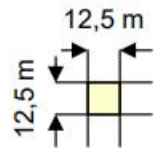
❖ GRD

Amplitude

8000

8210

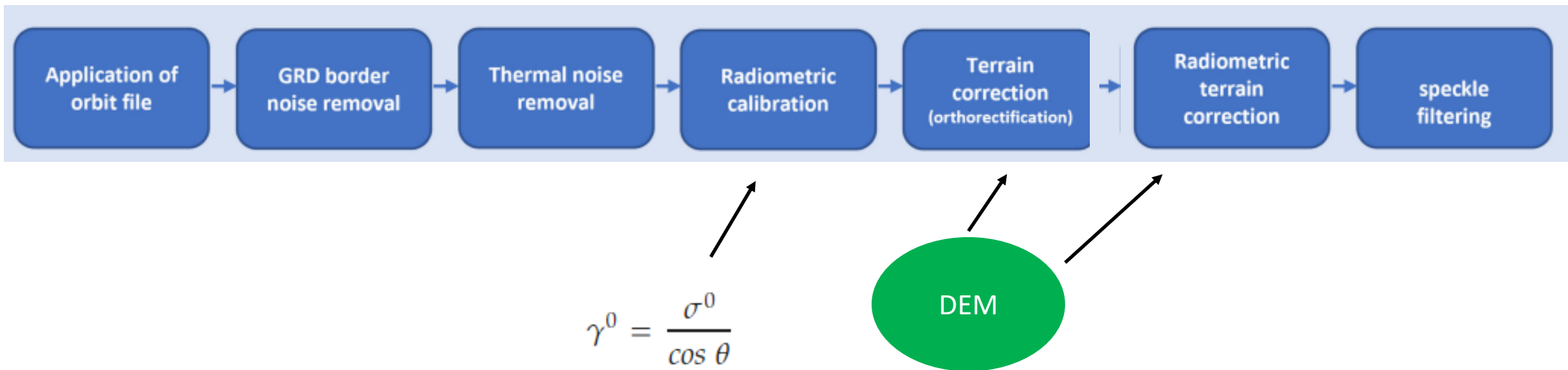
16 unsigned
bytes/pixel



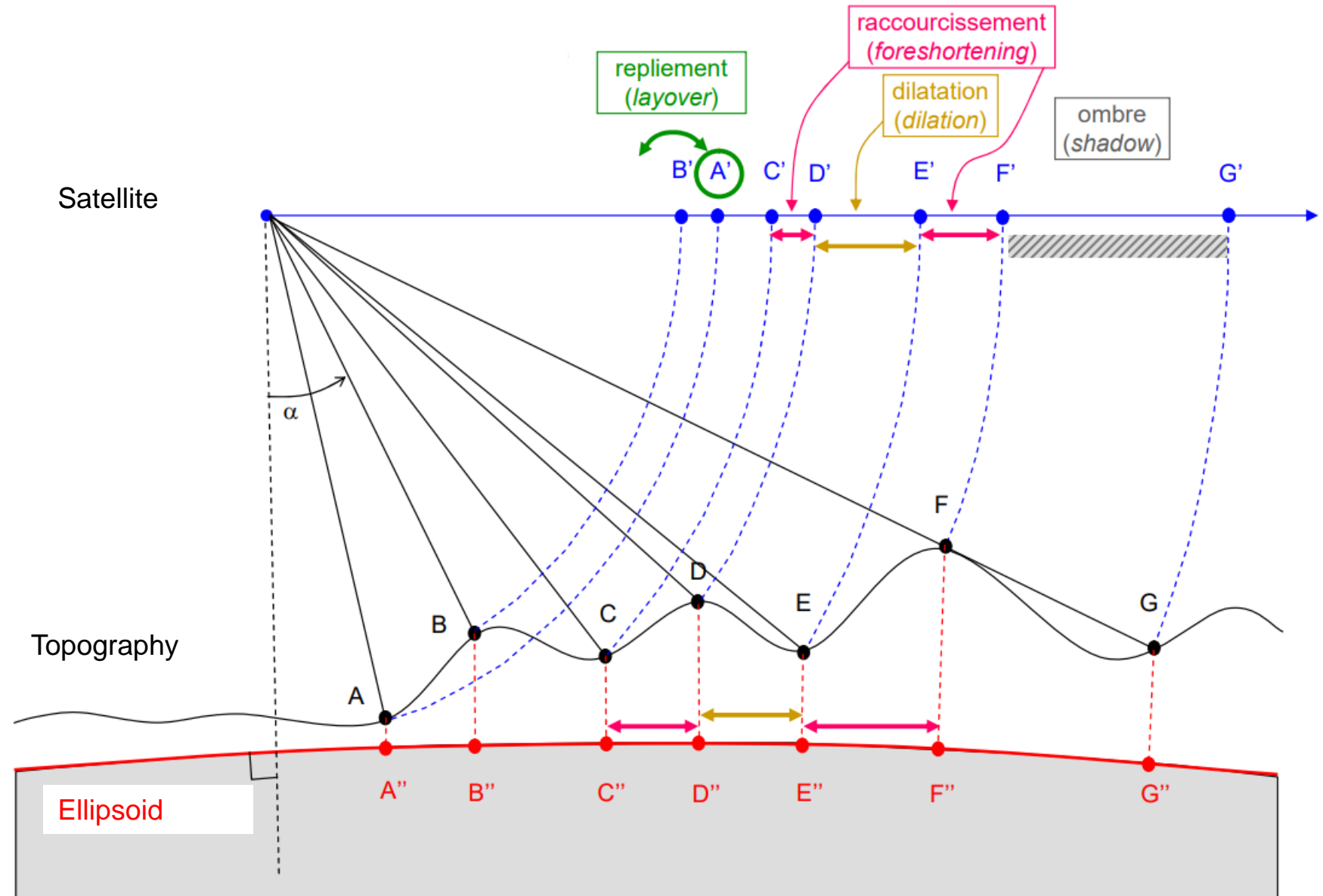
SAR images processing

Processing steps

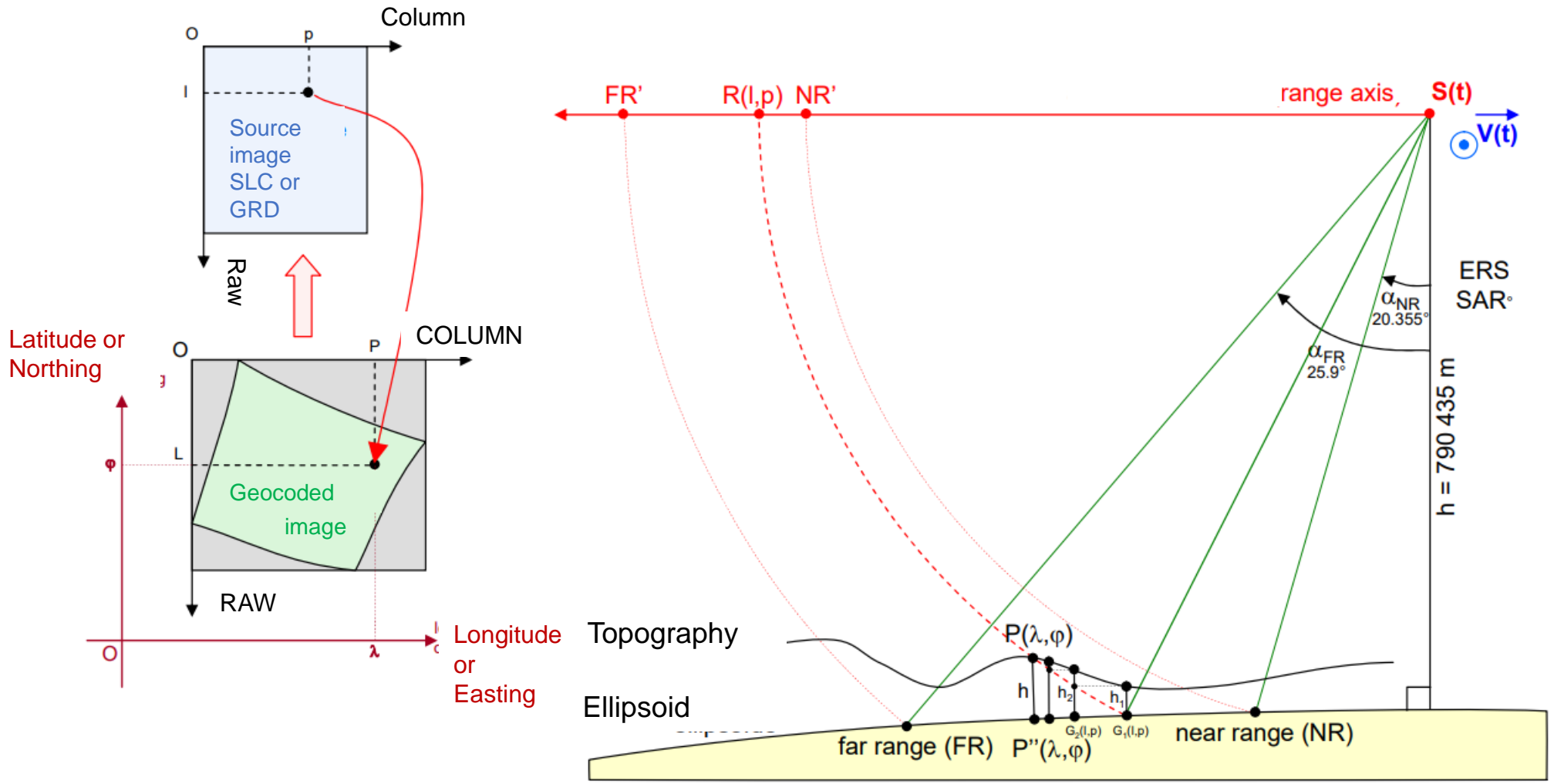
Adapted from Marzi & Gamba (2021)



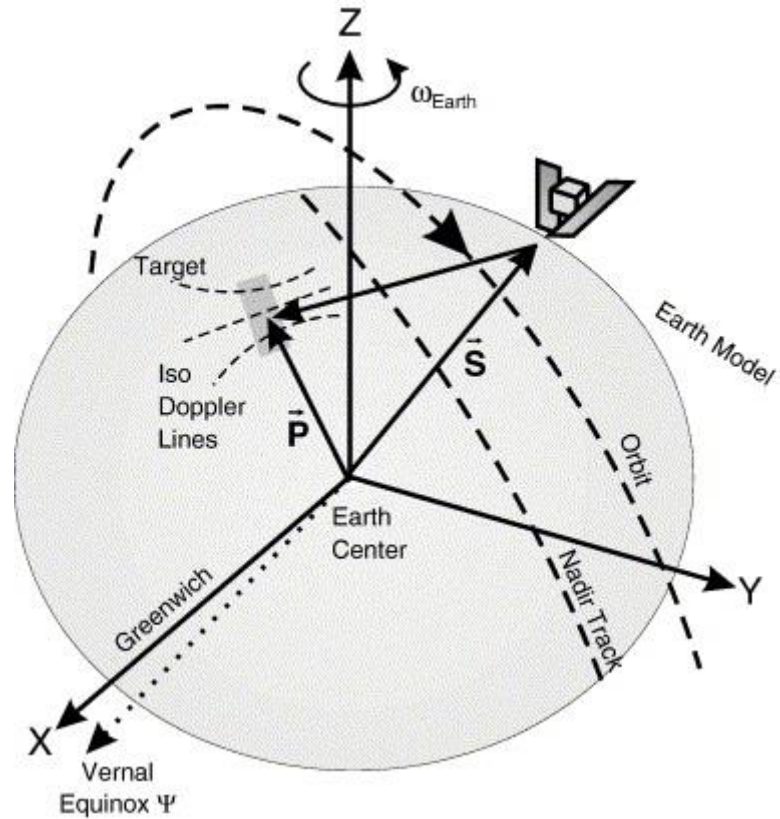
Geometry defaults



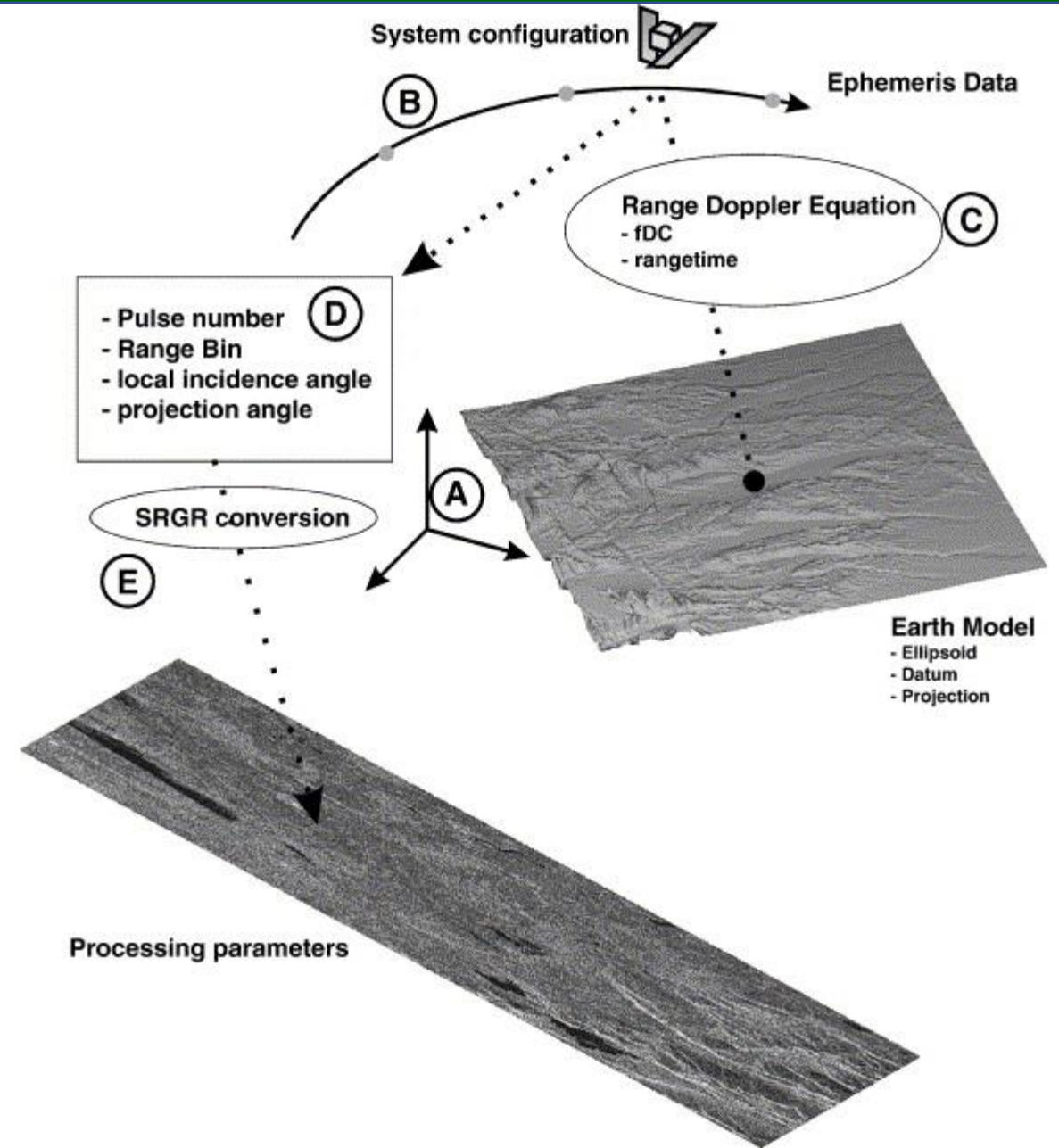
Orthorectification



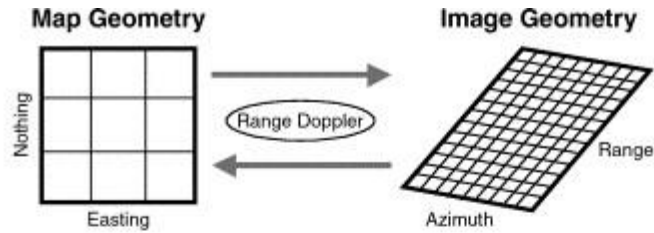
Precise geocoding



Loew & Mauzer (2007)



Radiometric normalization



A

$$A_{r,a} = \sin(\theta)^{-1}$$

$$\sigma^0(E, N) \xleftarrow{\sigma_{E,N}^0 \propto \int \sigma_{r,a}^0} \sigma^0(r, a) = \beta^0(r, a) \cdot \sin_{r,a}(\theta)^{-1}$$

Simple sin correction

B

$$\sigma^0(E, N) \xleftarrow{\sigma_{E,N}^0 \propto \int \sigma_{r,a}^0} \sigma^0(r, a) = \beta^0(r, a) / A_{r,a}$$

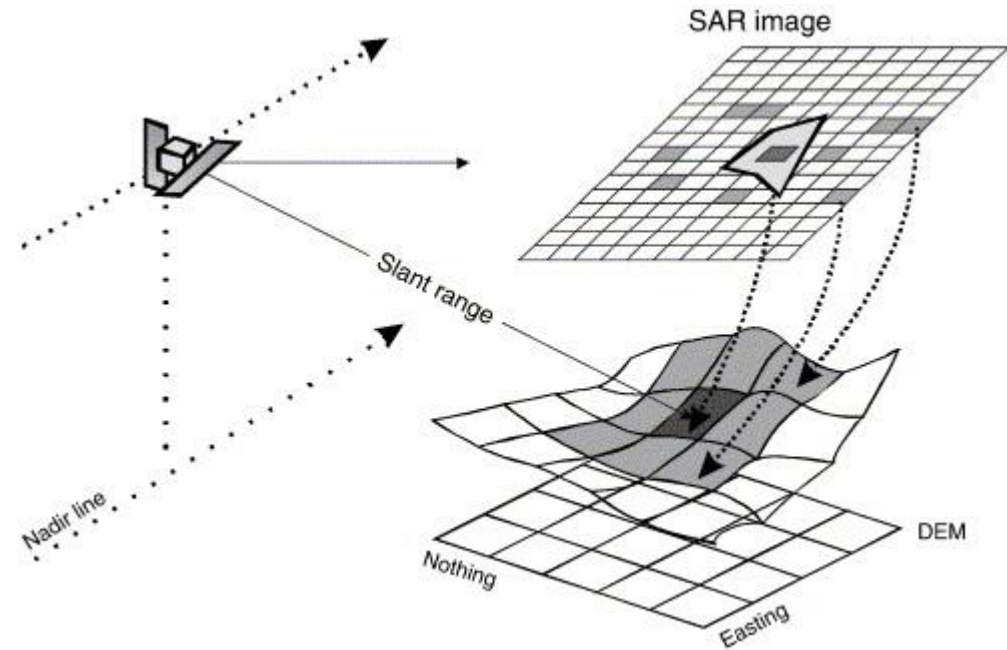
Facet method

C

$$A_{E,N} = \cos(\psi)^{-1}$$

$$\sigma^0(E, N) = \beta_{E,N}^0 \cdot \cos(\psi) \xleftarrow{\beta_{E,N}^0 \propto \int \beta_{r,a}^0} \beta^0(r, a)$$

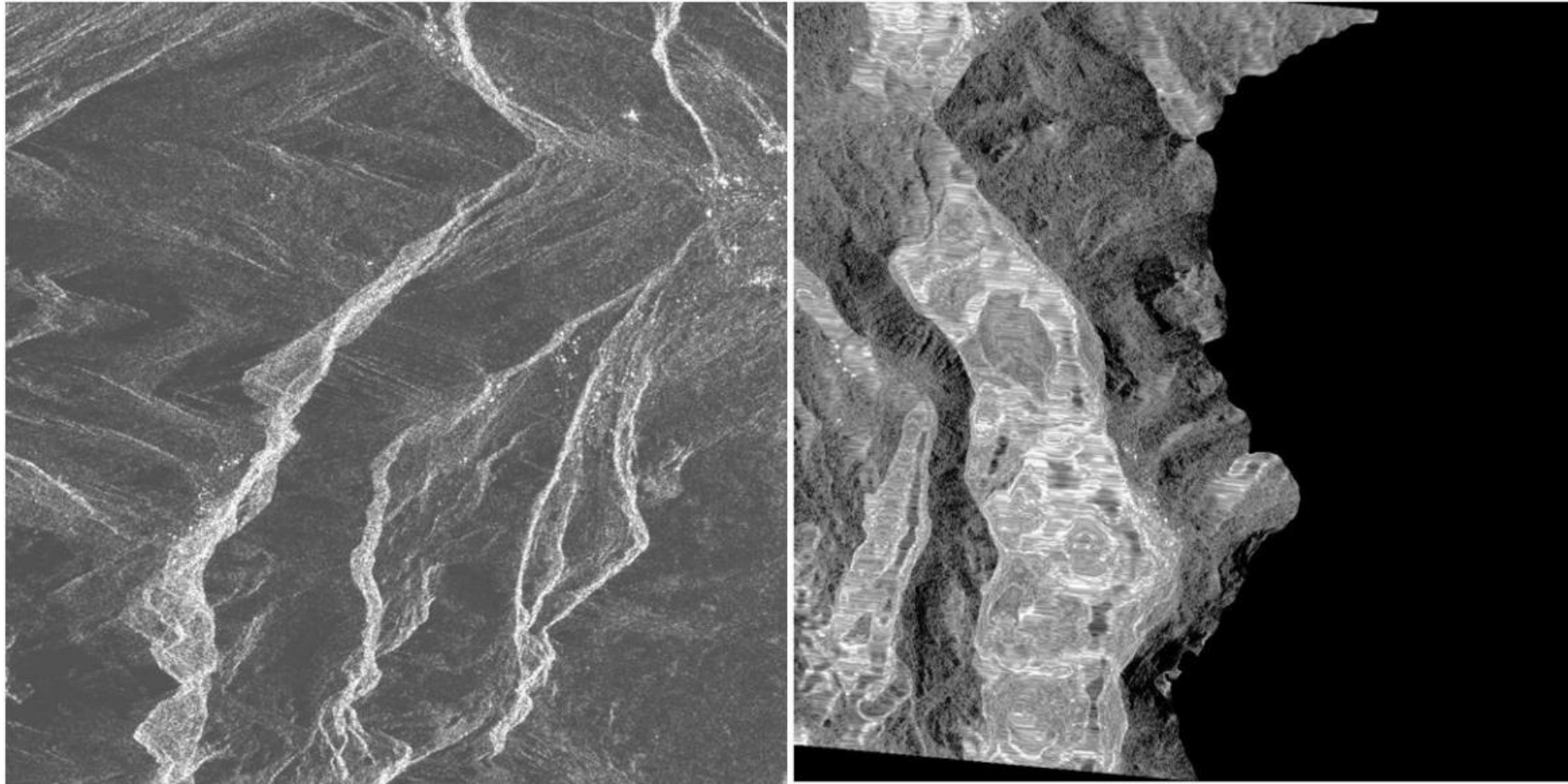
Brightness integration



Loew, A., & Mauser, W. (2007). Generation of geometrically and radiometrically terrain corrected SAR image products. *Remote Sensing of Environment*, 106(3), 337-349, doi:10.1016/j.rse.2006.09.002

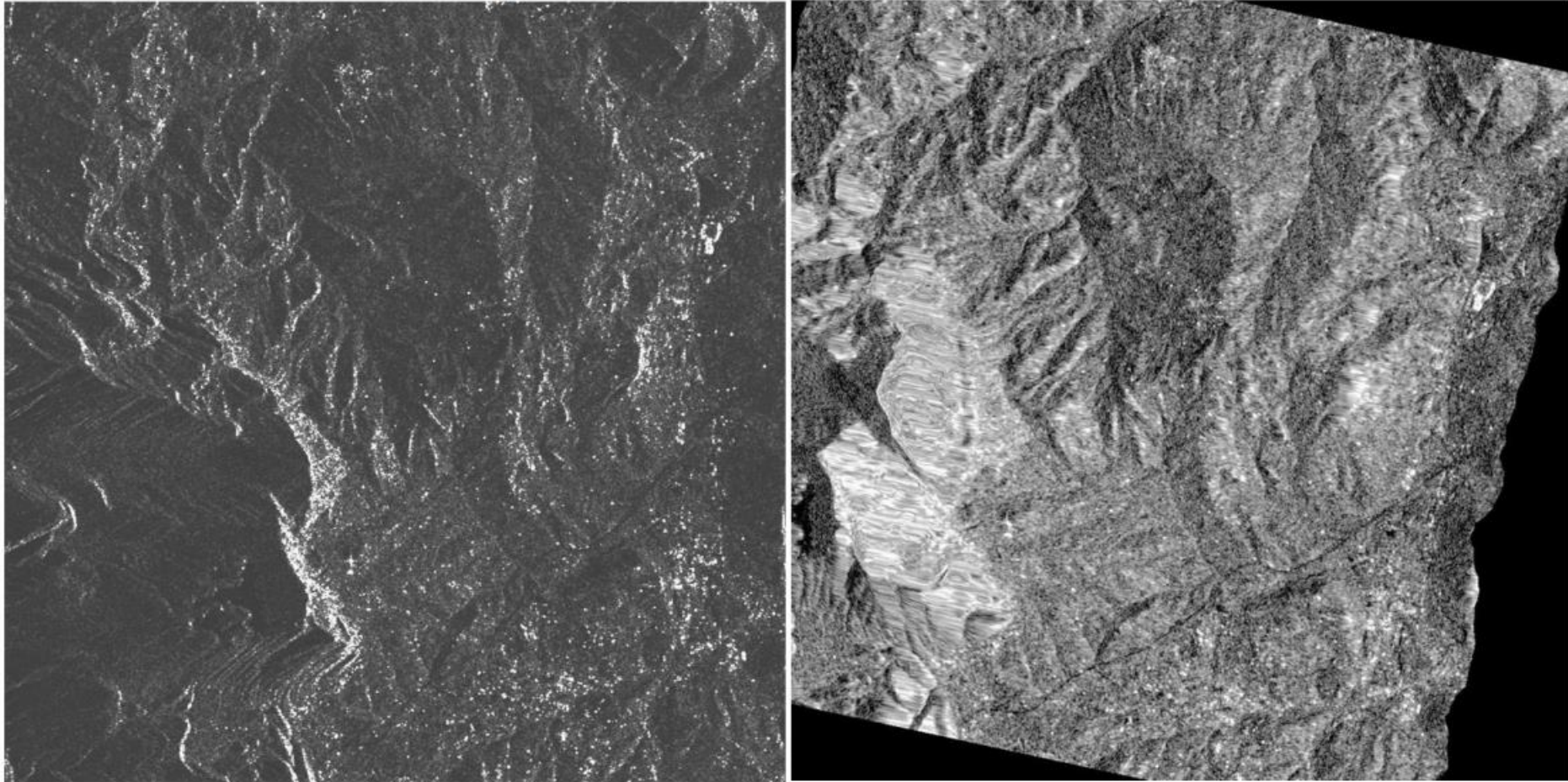
Orthorectification - examples

Alp mountains (France)



Orthorectification - examples

Napoli region(Italy)



Speckle noise

Speckle, appearing in synthetic aperture radar (SAR) images as granular noise, is due to the interference of waves reflected from many elementary scatterers. Speckle in SAR images complicates the image interpretation problem by reducing the effectiveness of image segmentation and classification (Lee et al., 1994).

Example of speckle on Sentinel-1 image from 27/09/2018 at the mouth of the Leyre River (Gironde, France) presented in Brodu (2018)



Lee J.S., Jurkevich L., Dewaele P., Wambacq P., Oosterlinck A. (1994). Speckle filtering of synthetic aperture radar images: A review. *Remote Sensing Reviews*, 8(4), 313-340, doi:10.1080/02757259409532206.

Speckle noise

- Spatial filters:

A. Box Filter (Mean Filter)

The box filter is a convolution filter that replaces the center pixel by the mean value of pixels in a square filtering window. Although it has a good speckle smoothing ability, it shows very poor performances in preserving spatial resolution and it alters coarsely the polarimetric parameters (entropy, coherence...). Because Box filter is an indiscriminating filter, small window sizes, 3x3 or 5x5, should be applied for filtering in order to lessen these issues.

B. Enhanced Lee Filter

The enhanced Lee filter [1] is an adaptive filter based on the estimation of the local variance statistics. The adaptive filtering weights are determined using the span image that benefits from the scattering characteristics of the HH, VV and HV intensities. The filter does not use the standard square filtering window, but an edge-aligned window with the aim of preserving edges and details features. Among eight possibilities, a non-square window is selected dependently on the edge direction detection with respect to the center pixel. The edge direction is realized by an edge mask using the submeans of 3x3 subwindows. Once the window has been chosen, the local statistics are estimated from which the local linear minimum mean-square filter is obtained,

$$\hat{x} = \bar{y} + b(y - \bar{y}) \quad (4)$$

where \hat{x} is the filtered pixel value, \bar{y} is the local mean, and b weighting function such as

$$b = \frac{\text{var}(x)}{\text{var}(y)} \quad \text{and} \quad \text{var}(x) = \frac{\text{var}(y) - \bar{y}^2 \sigma_v^2}{(1 + \sigma_v^2)} \quad (5)$$

where σ_v^2 is the noise variance. Finally the same weight parameter b , computed from (5), is used similarly to filter each element of the covariance matrix C .

preset threshold η . That threshold is defined as some percentage of the sum of all the eigenvalues. Then the estimated parameter vector \hat{p} is rebuilt only with the "signal subspace".

$$\hat{p} = \mu_p + Q_S Q_S^T (p - \mu_p) \quad (7)$$

Finally, the filtered Mueller matrix can be extracted from the first nine elements of the estimated parameter vector.

D. Speckle Reducing Anisotropic Diffusion (SRAD) Yu Filter

The SRAD method [8] is a Partial Differential Equations (PDE) filtering algorithm that regularizes iteratively an image. During each iteration t , the image I is updated at each pixel position (x, y) according to the following PDE

$$\frac{\partial I(x, y, t)}{\partial t} = \text{div}(c(q)\nabla I(x, y, t)) \quad (8)$$

where ∇ is the gradient operator, div is the divergence operator, q is the *Instantaneous Coefficient Of Variation* (ICOV) and $c()$ is the diffusion coefficient function that acts as an "edge stopping" function. The $c()$ function (9) lessens the diffusion process when ICOV becomes higher than the speckle noise level $q_0(t)$.

$$c(x, y, t) = \frac{1}{1 + \left[q^2(x, y, t) - q_0^2(t) \right] \sqrt{\left[q_0^2(t) \right] (1 + q_0^2(t))}} \quad (9)$$

At each iteration, $q_0(t)$ has to be determined within an homogeneous area. The coefficient of diffusion are computed on the span and then are applied on the others elements of the polarimetric covariance matrix, or the polarimetric coherency matrix.

C. Subspace Filter

The purpose of this technique [7] consists in decomposing in subspaces a parameter vector, which characterizes a pixel. The parameter vector p of each pixel is composed of 10 parameters. The first nine are generated from the Mueller matrix and the tenth one is the weighted entropy value. First, it is necessary to apply a square scanning window to get the local covariance matrix C_p of the parameter vector,

$$C_p = E \left\{ (p - \mu_p)(p - \mu_p)^T \right\} = Q \Lambda Q^T, \quad \text{and} \quad Q = (Q_S | Q_N) \quad (6)$$

where μ_p is mean vector of the parameter vectors p in the scanning window, Q and Λ are respectively the eigenvectors and eigenvalues matrix of C_p . By assuming that there exist m ($m < 10$) different target signals in the area to be filtered, the signal is divided in two orthogonal subspaces. The m -dimensional subspace is the "signal space" Q_S , i.e the m first eigenvectors, whereas the $(10-m)$ -dimensional subspace is called "noise subspace" Q_N , which is due to speckle effect. The rank m of the "signal subspace" corresponds to the minimum number of eigenvalues required so that their sum is larger than a

E. Trace Based Partial Differential Equation Filter

The trace-based [9] filter is a PDE filter that is equivalent to a local convolution by oriented Gaussian filters. The regularization process is driven by the PDE(10).

$$\frac{\partial I(x, y, t)}{\partial t} = \text{trace}(\mathbf{D}\mathbf{H}) \quad (10)$$

where \mathbf{D} is the diffusion tensor, and \mathbf{H} is the local image hessian.

F. Scattering Model Based Filter(SMB)

The first stage of this filter [10] consists of applying a Freeman - Durden decomposition [11] on the polarimetric data. The pixels are assigned to dominant scattering mechanism category, which are one of the three: surface scattering, volume scattering, double bounce scattering mechanism. For single look images, it is necessary to realize a multilooking in azimuth until we reach an equivalent number of look of 3, otherwise an averaging window 3x3 is needed to calculate the dominant scattering mechanism. Then each set of pixels attributed to a category is divided equitably into 30 clusters, or more. Next, for each category we merge two clusters according to a merge distance measurement, until we reach n desired final classes. Afterward, all pixels are classified based on their

distance of Wishart computed with respect to the centers of classes V_m .

$$d(C, V_m) = \ln|V_m| + \text{Tr}(V_m^{-1}C) \quad (11)$$

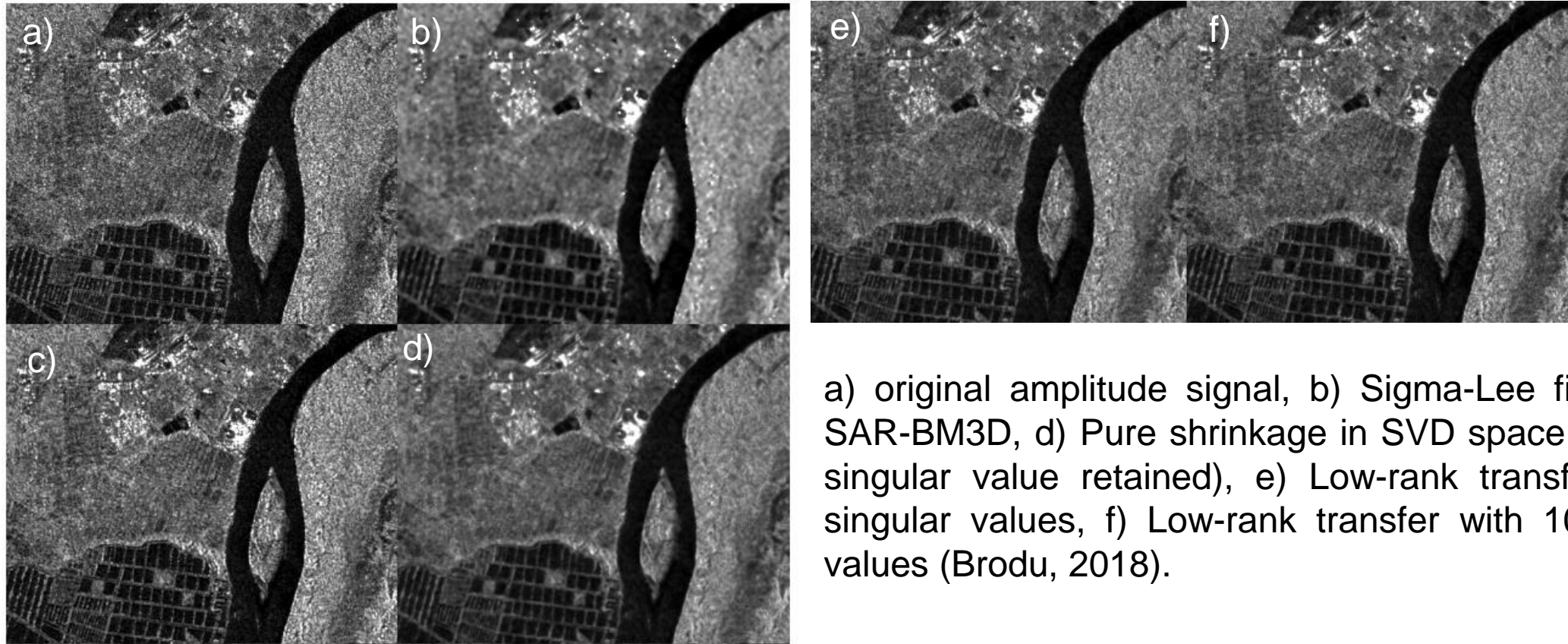
$$C \in V_m \text{ if } d(C, V_m) \leq d(C, V_j), \forall j \neq m$$

To reach a better convergence, it is preferable to apply repetitively classification of Wishart 4 times. Finally, the pixel in the center of a window of 9x9 is filtered but only using the pixels of the same class of the central pixel and the pixels which belong to two classes close to the same category. Pixels of the brightest classes for the surface and double bounce category are not filtered. Pixels belonging to the darkest or brightest classes of a category are filtered only with pixels of the same class. The filter is based on the minimization of the error quadratic, as in the enhanced Lee filter [1]. Moreover, if the quantity of pixels in filtering window 9x9 is less than 5, then we include the neighboring pixels in a 3x3 scanning window to filter.

Speckle noise

- Temporal filters: similar techniques as for the spatial domain.

Spatial/temporal filtering \Rightarrow degradation of spatial/temporal resolution



a) original amplitude signal, b) Sigma-Lee filtering, c) SAR-BM3D, d) Pure shrinkage in SVD space (only one singular value retained), e) Low-rank transfer with 5 singular values, f) Low-rank transfer with 10 singular values (Brodu, 2018).

Brodu N. (2018). Low-rankness transfer for denoising Sentinel-1 SAR images. *9th International Symposium on Signal, Image, Video and Communications (ISIVC)*, 106-111.